Materials Characterization 142 (2018) 115–123

Contents lists available at ScienceDirect

Materials Characterization

journal homepage: www.elsevier.com/locate/matchar

Effect of grain boundary character distribution on weld heat-affected zone liquation cracking behavior of AISI 316Ti austenitic stainless steel

RamReddy K, Nandha Kumar E, R. Jeyaraam, G.D. Janaki Ram, V. Subramanya Sarma*

Department of Metallurgical and Materials Engineering, Indian Institute of Technology Madras, Chennai 600036, India

ARTICLE INFO

Keywords:
Grain boundaries
Welding
Liquation cracking
Thermomechanical processing
Special boundaries
Varestraint testing
316Ti austenitic stainless steel

ABSTRACT

In this work, the role of grain boundary engineering (GBE) on the weld heat-affected-zone (HAZ) liquation cracking resistance of austenitic stainless steel AISI 316Ti was investigated. Standard wrought-processed alloy 316Ti was cold rolled to 5% strain and subsequently annealed at 1373 K for 30 min to achieve the optimum grain boundary character distribution (GBCD). The GBE samples were found to consist of a significantly higher fraction (72%) of low Σ coincident site lattice (CSL) boundaries as compared to the as received (AR) samples (45%). To study the liquation cracking behavior, single-track longitudinal varestraint tests was performed on AR and GBE samples. Microstructural examination revealed that the grain coarsening and the liquation events were less prominent in the GBE samples as compared to the AR samples. It is believed that the reduced segregation of impurities to the special boundaries (coherent Σ3 twins, in particular) present in the GBE samples is responsible for the observed improvement in the HAZ liquation cracking resistance.

1. Introduction

Weld heat-affected zone (HAZ) liquation cracking is a major problem in fusion welding of stabilized grades of austenitic stainless steels such as AISI 316Ti. Liquation cracking occurs due to formation of continuous liquid films along the grain boundaries, often caused by segregation of impurities and/or constitutional liquation of carbides and carbosulfides [1–3]. Studies by Shankar et al. [1] show that stabilized grades of austenitic stainless steels (containing Ti or Nb) are more prone to HAZ liquation cracking than non-stabilized grades. Given that liquation cracking is essentially a grain boundary phenomenon, it should be possible to overcome the problem by modifying the nature of grain boundaries [4]. Watanabe [5] originally introduced the concept of grain boundary engineering (GBE) to improve the physical and mechanical properties of polycrystalline materials by altering the grain boundary character and distribution [5]. GBE aims to achieve, through appropriate thermo-mechanical processing of the material, a high fraction of coincident site lattice (CSL) boundaries with $\Sigma \leq 29$. The CSL boundaries with $\Sigma \leq 29$, often referred to as "special boundaries", are characterized by lower energy, lower mobility and higher atomic packing as compared to random high angle grain boundaries (HAGBs) [6,7]. Through GBE, several investigators have demonstrated significant improvements in resistance to creep [8], fatigue [9], intergranular corrosion [10,11], stress corrosion cracking [12], hot corrosion [13], and embrittlement [14]. Further, Lehockey et al. [4] observed significant improvement in strain-age cracking resistance of Ni and Fe based superalloys by GBE. More recently, Qian and Lippold [15] studied the effects of special boundaries on HAZ liquation cracking in a Ni base superalloy and reported a significant improvement in resistance to cracking with increasing special boundary fraction. The present investigation aims to verify whether a similar improvement in HAZ liquation cracking resistance can be achieved in austenitic stainless steel AISI 316Ti by optimizing its grain boundary character distribution (GBCD).

2. Materials and Methods

A wrought processed austenitic stainless steel AISI 316Ti plate of 6.5 mm thickness was used as as-received (AR) material. The chemical composition of the base plate as determined by optical emission spectroscopy (OES) (Spectrolab model, Ametek make) is given in Table 1. For modifying the GBCD, small strips cut from the base plate (along the rolling direction) were thermomechanically processed (TMP) as detailed in Table 2. Samples for optical microscopy and scanning electron microscopy (SEM) were prepared as per standard metallographic procedures. Etching was done electrolytically using 10% oxalic acid with Pt cathode and stainless steel anode at 1.5 V and 1 A cm^{-2} current density for 15 s. For measurements of GBCD in AR and TMP samples, electron backscattered diffraction (EBSD) analysis was carried out. Samples for EBSD analysis were prepared by electrolytic polishing using

* Corresponding author.
E-mail addresses: jram@iitm.ac.in (J.R. G.D.), vsarma@iitm.ac.in (S.S. V.).

https://doi.org/10.1016/j.matchar.2018.05.020
Received 17 February 2018; Received in revised form 30 April 2018; Accepted 13 May 2018
Available online 18 May 2018

Table 1
Chemical composition (in wt%) of 316Ti stainless steel by optical emission spectroscopy.

Element	C	Cr	Ni	Mo	Mn	Ti	Si	Cu	P	S	N	Fe
Wt%	0.04	18	13.2	2.3	1.86	0.52	0.46	0.31	0.022	0.015	0.012	Rest

Table 2
Various thermomechanical processing schedules employed in GBE optimization.

Deformation (%)	Temperature (K)	Time (hours)
As received (no prestrain)	1273	0.5& 1
	1323	0.5& 1
	1373	0.5& 1
5% prestrain	1273	0.5& 1
	1323	0.5& 1
	1373	0.5& 1
10% prestrain	1323	0.5& 1

a solution of 6% perchloric acid, 60% methanol, and 34% butoxyethanol at ambient temperature at 20 V for 30 s after conventional metallographic polishing. EBSD was performed using field emission scanning electron microscope (Inspect F model, FEI make) with Hikari high-speed camera using TSL-OIM™ data acquisition system (version 7.2.1) and post processing software (EBSD parameters: 1 μm step size, 20 kV voltage, 150 μA emission current). To ensure sufficient statistics, at least three or more scans of 500 × 500 μm^2 were performed on each specimen and the data reported in this article is the average value obtained from these scans. To identify CSL boundaries, Brandon's criterion [7] is used. Random high angle grain boundaries (HAGBs) are defined as the boundaries with misorientation angle $\theta > 15^\circ$ and are not low Σ (≤29) CSL boundaries. Grain size was measured using linear-intercept method (average of horizontal and vertical intercept lengths) and a misorientation angle of 5° was used as the cut off for evaluating the grain size. Grain size was measured with and without considering twins as grain boundaries. The EBSD data sets were further analyzed to determine the triple junction distributions in all the processed specimens. There are essentially four types of triple junctions, namely 0-CSL, 1-CSL, 2-CSL and 3-CSL (n-CSL refers to a triple junction having "n" number of CSL boundaries at the intersection). The triple junction distribution analysis was carried out by exporting the triple junction data using TSL-OIM™ software to a customized computer program and calculating the fraction of n-ΣCSL (Σ ≤ 29) boundaries present.

Longitudinal varestraint tests were carried out on AR and GBE samples (125 × 25 × 3 mm) to assess their hot cracking behavior. The welding parameters are listed in Table 3. Two different augmented strain levels were used (2% and 4%). At each strain level, six samples were tested in each condition (AR and GBE). After testing, the specimens were cleaned and examined under a stereomicroscope. Only the cracks present in the HAZ of the varestraint test welds were considered for analysis. The total number of cracks, maximum crack length (MCL) and total crack length (TCL) were evaluated. Samples cut from the varestraint test regions (top surface) were also prepared for EBSD examination. Using the same welding parameters as listed in Table 3, a few bead-on-plate welds were also produced in AR and GBE samples for microstructural analysis in different weld regions.

Table 3
Welding parameters.

Parameter	Varestraint testing
Current, Amp	80
Voltage, Volts	10–15
Travel speed, mm/s	3.5
Arc gap, mm	1.8
Shielding gas, lpm	CP argon, 18
Die radius, inches (augmented strain)	1.56(~4%), 3.12 (~2%)

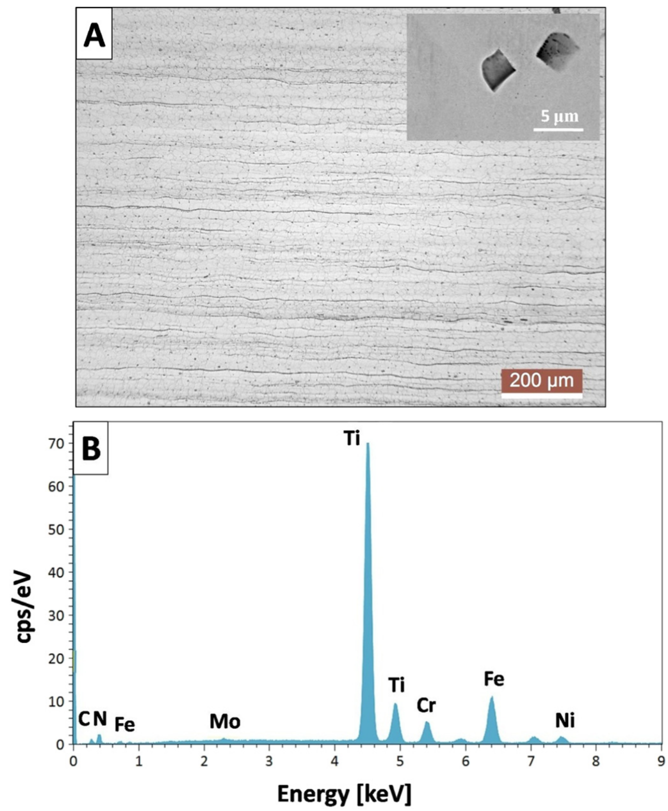

Fig. 1. A) Optical micrograph showing ferrite stringers in AR material (Inset shows higher magnification image of (Ti, Mo) carbide particles). B) EDS spectra of (Ti, Mo) C particles in AR material.

3. Results and Discussion

3.1. Base Material Microstructure

Microstructural examination of alloy 316Ti base plate in AR condition revealed equiaxed grains with the presence of δ-ferrite stringers (Fig. 1a). Energy dispersive spectroscopy (EDS) studies on the base material indicated the presence of Ti, Mo based carbides/carbonitrides (Fig. 1b). The inverse pole figure (IPF) map shows equiaxed grains and the phase map indicates presence of γ and δ-Fe in AR sample (Fig. 2). From EBSD data, the average grain size of the AR sample was estimated to be 6 μm considering twins as grain boundaries and 10 μm without considering twins as grain boundaries (Fig. 2a). The stringers seen in optical microscopy (Fig. 1) were identified to be δ-ferrite phase by EBSD (Fig. 2b). These delta ferrite stringers are located at the austenite grain boundaries and are discontinuous.

3.2. Optimization of Grain Boundary Character Distribution

To generate the microstructure with optimized grain boundary character distribution (GBCD) (hereafter referred to as GBE microstructure) the AR material was subjected to GBE treatments which